 AIAA 2013-2188

Correlation of Irrotational Near-field Pressure and Far-field Acoustic in Forced High-Speed Jets

M. Crawley[1], H. Alkandry[2], A. Sinha[3] and M. Samimy[4]
Gas Dynamics and Turbulence Laboratory
Aeronautical and Astronautical Research Laboratories
Department of Mechanical and Aerospace Engineering, The Ohio State University
2300 West Case Road
Columbus, Ohio 43235-7531 USA

The near-field pressure of a Mach 0.9 jet with Reynolds number of 6.2×10^5 has been investigated in order to characterize the hydrodynamic and acoustic response to low-frequency forcing with localized arc filament plasma actuators. Simultaneous acquisition of the far-field acoustic, the near-field pressure, and the actuation phase enables the use of phase-averaging of the pressure and acoustic signals and space-time correlations between the near field and the far field. Results show that forcing at very low frequencies results in structures that evolve independently as they advect through the shear layer. As the forcing frequency is increased, the structures begin to interact quasi-linearly. Autocorrelations of the phase-averaged near field signals show coherent acoustic radiation, indicating that the coherent large-scale structures generate coherent acoustic radiation. The interaction and potential disintegration of the large-scale structures as they pass through the end of the potential core has been suggested as a source mechanism for downstream acoustic radiation; the results of this study also point towards this mechanism as being the dominant noise source towards the downstream polar angles in this jet.

Nomenclature

a_∞	=	Ambient speed of sound (m/s)
D	=	Nozzle exit diameter (m)
U_j	=	Nozzle exit velocity (m/s)
U_c	=	Convective velocity for large-scale structures (m/s)
f	=	Spectral frequency (Hz)
f_F	=	Forcing frequency (Hz)
R	=	Distance from near-field microphone to far-field microphone (m)
Re_D	=	Reynolds number based on D and nozzle exit conditions
St_{DF}	=	Forcing Strouhal number ($f_F D/U_j$)
y	=	Radial coordinate normal to the jet axis (m)

I. Introduction

The acoustic radiation from commercial and military jets has long been an issue for aircraft engine manufacturers and operators. The escalating number of flights, encroachment of urban and residential areas near airports, and tightening of environmental regulations have forced airport managers to introduce costly curfews, surcharges, flight path restrictions, and other measures to reduce noise levels in and around airports. It was shown by Lighthill[1] that the acoustic radiation emitted by a jet scales with the eighth power of the jet exit velocity, U_j, and with the second power of the jet diameter, D. As the jet thrust scales with the second power of both the jet exit velocity and jet diameter, the problem of jet noise was initially tackled by designing engines with large bypass ratios. The large nozzle diameters and lower jet exit velocities minimized the acoustic radiation while preserving the generated thrust, with the added benefit of significantly increased fuel efficiency. With engine diameters reaching the limit for what can be installed on airframe designs currently used by aircraft manufacturers, engine designers must confront the challenge of jet noise by a different approach. Additionally, large bypass ratio engines are not suitable for supersonic civilian or military aircraft, where low drag is necessary. Implementation of flow control

[1] Graduate Research Assistant, AIAA Member
[2] Graduate Research Assistant, AIAA Member
[3] Currently, Postdoctoral Scholar at California Institute of Technology, AIAA Member
[4] Nordholt Professor, AIAA Fellow, Corresponding Author, Samimy.1@osu.edu

strategies, either passive or active, is necessary in order to meet future aircraft regulations as well as the performance requirements.

Many techniques to reduce the acoustic radiation from high-speed jets using either passive or active modifications to the nozzle have been investigated, however these have primarily been in a trial-and-error fashion. This is because no consensus has yet formed in the aeroacoustic community over the precise mechanism by which subsonically convecting coherent structures generate sound, despite decades of work. Major issues arise due to the non-uniqueness of potential source models: a given far-field acoustic pattern can be generated by any number of multipole distributions. Hence, to determine the causal relationship between the turbulent eddies in the flow and the far-field acoustic radiation, the near field of the jet must also be probed. In the present work the irrotational near-field pressure and acoustic far field of high Reynolds number, high Mach number jets excited with localized arc-filament plasma actuators (LAFPAs) have been assayed, with the goal of improved understanding of the dynamics which lead to acoustic radiation from large-scale structures. Large-scale structures have been implicated as the dominant source of noise in high Mach number, subsonic jets, though the precise mechanism by which they produce acoustic radiation is currently not well understood[2,3]. To this end, microphones were positioned outside the jet shear layer, where they predominantly capture the linear hydrodynamic/acoustic pressure field that is produced by the large-scale structures while avoiding the nonlinear vorticity and entropy sources inside the shear layer[4,5]. The non-intrusive nature of the measurement technique is an added benefit. Excitation of the jet shear layers via LAFPAs has been shown to regularize the most prominent hydrodynamic perturbations in the shear layer[6-10], and hence the near-field pressure and acoustic radiation as well. Phase-averaging of the pressure signal can then be performed, based upon the period of excitation, helping to elucidate the near-field response of the jet to the large-scale structures.

II. Background

The composition of jet noise and the relative strength of the noise sources are highly dependent on the jet Mach number and temperature. Subsonic, unheated jet noise is dominated by mixing noise from the entire spectrum of turbulent scales in the jet shear layer. Highly directive in nature, mixing noise from large-scale structures radiates predominately towards the downstream jet axis. Sideline angle emission is dominated by small-scale turbulence, which is omni-directional and generated throughout the jet mixing layer[11,12]. In addition to the subsonic jet noise sources, supersonic jets can contain additional noise sources, namely Mach wave radiation, screech tones, and broadband shock-associated noise. Mach wave radiation is a major component of jets that are acoustically supersonic (i.e. $U_c/a_\infty > 1$, where U_c and a_∞ are the convective velocity of the large-scale structures and the ambient speed of sound, respectively), and is generated by the supersonically convecting large-scale structures in the turbulent shear layer relative to the ambient speed of sound[13]. Additionally, mathematical models of the growth, saturation, and decay of the large-scale structures have shown frequency broadening which results in a portion of the structure energy obtaining supersonic phase velocities, even in cases where the actual large-scale structure had a subsonic velocity[14].

The generation and evolution of the large-scale structures in the jet shear layer are dependent on two types of instabilities inherent in axisymmetric jets: the initial shear layer instability and the jet column or preferred mode instability. In addition, axisymmetric jets possess azimuthal modal content, which has significant effect on the development of flow structures as well as the radiated noise. Additional information on the jet instabilities and how they affect the development of the jet and the emitted acoustic radiation thereof can be found in the references[6,15-22]. Numerous techniques to control the development of the large-scale structures, and hence acoustic radiation control, in jets have been devised and can be divided into two main categories: passive and active control techniques. Examples of passive techniques are chevrons, tabs, and lobed mixers, which rely on generating streamwise vorticity to increase mixing in the near nozzle region, thus reducing the strength of the large-scale structures[23,24]. Active flow control techniques are desirable as they present benefits over their passive counterparts - the most obvious of which is that they can be disabled when unnecessary, so that any parasitic effects of the control technique are not present during all flight regimes of the aircraft. However, challenges remain in implementing active techniques in jets of interest, where the high Reynolds number and Mach number require high amplitude, high frequency actuators. Acoustic drivers, which were a mainstay of active flow controllers in laboratory environments as they have control authority over high subsonic jets when forced around the jet preferred mode[25-28], have been shown to lose their control authority as the Mach number and Reynolds number increased as well as at higher frequencies required to force the jet initial shear layer instabilities.

The Gas Dynamics and Turbulence Laboratory (GDTL) has developed a class of plasma actuators, referred to as localized arc filament plasma actuators (LAFPAs), which can provide excitation signals of high amplitude and high frequency required for control of high Mach number and Reynolds number jets[29,30]. GDTL has used these actuators

for noise mitigation and flow control in Mach 0.9[22,31], Mach 1.3[6,8,32,33] and Mach 1.65[34] unheated jets, and has recently expanded the use of LAFPAs to heated jets. A review of the development of LAFPAs and their use in flow control and fluid phenomena research in high speed, high Reynolds number jets, both heated and unheated, can be found in Samimy et al.[35]. Recently, the diagnostic potential of LAFPAs for understanding jet flow phenomena has been explored. Excitation of the flow by LAFPAs results in a definitive spatio-temporal origin to which resulting phenomena can be referenced. The absolute temporal reference afforded by LAFPA excitation provides researchers the ability to investigate the growth, saturation, and decay of structures with high fidelity. Kearney-Fischer et al.[13] investigated Mach wave radiation from heated, high Mach number jets using schlieren imaging phase-locked to LAFPAs, among other data acquisition techniques. Sinha et al.[10] showed the quasi-linearity of large-scale structure interaction through phase-averaging of the near-field pressure in jets forced at low Strouhal numbers ($St_{DF} < 0.5$).

III. Experimental Methodology

All experiments were conducted at the GDTL within the Aeronautical and Astronautical Research Laboratories at the Ohio State University. Compressed, dried, and filtered air is supplied to the facility from two cylindrical storage tanks with a total capacity of 43 m^3 and maximum storage pressure of 16 MPa. The air may be routed through a storage heater (not used in this study), which allows the jet to operate with a stagnation temperature up to 500 °C, before expanding through a nozzle and exhausting horizontally into an anechoic chamber. Opposite the nozzle, a collector accumulates the entrained air from the jet and exhausts it to the outdoors. A schematic of the anechoic chamber can be seen in Figure 1. The dimensions of the chamber are 6.20 m wide by 5.59 m long and 3.36 m tall, with internal wedge-tip to wedge-tip dimensions of 5.14 m by 4.48 m and 2.53 m, respectively. The design of the chamber produces a cutoff frequency of 160 Hz, well below the frequencies of interest. A more detailed description of the GDTL anechoic chamber properties and validation has been given by Hahn[36].

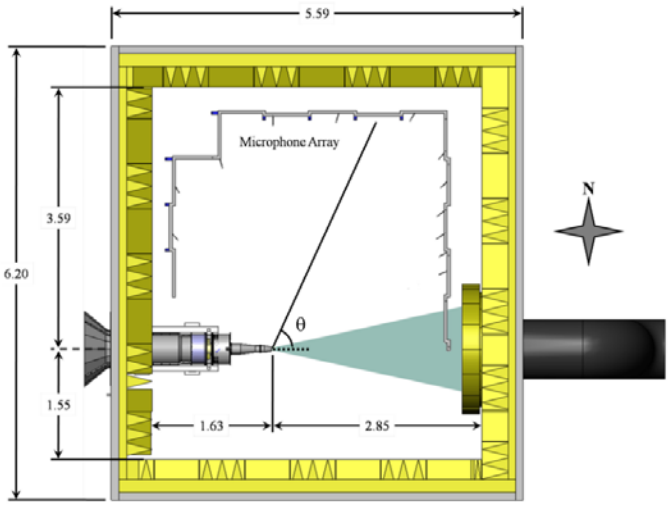

Figure 1: Plan view of the anechoic chamber at the GDTL (dimensions in meters).

For this study a converging, axisymmetric nozzle with exit diameter D of 25.4 mm (1 in.) was used. The internal contour of the nozzle was designed using a fifth order polynomial. The nozzle utilized a thick-lipped design in order to simplify the mounts for the extension, which housed the eight actuators used in this study. For the experiments reported in this paper, the jet was operated at a Mach number (M_j) of 0.90, and with a total temperature ratio of unity. The Reynolds number based on the jet exit diameter was 6.2×10^5; previous investigations using hot-wire anemometry have indicated that the initial shear layer is turbulent for this operating condition with momentum thickness ~0.09 mm and displacement thickness ~1.2 mm[7].

A. Localized Arc Filament Plasma Actuators

Each LAFPA consists of a pair of tungsten pin electrodes, which are placed around the nozzle perimeter 1 mm upstream of the nozzle exit. Eight uniformly spaced actuators were used in this study. The center-to-center spacing between electrode pairs for each actuator is 4 mm. The electrodes are housed in a boron nitride extension attached to the end of the nozzle. A groove with dimensions 1 mm wide and 0.5 mm deep is machined in the boron nitride, into which the electrode tips protrude, to provide a region of low momentum flow in order to stabilize the formation of

the plasma arcs. It has been shown that the existence of this groove does not substantially alter the flow field or the control authority of the LAFPAs[37]. A more detailed description of LAFPA characteristics can be found in Utkin et al.[30].

The LAFPAs are energized by a multi-channel, high-voltage plasma power generator capable of simultaneously powering up to eight LAFPAs, which was designed and built in-house at the GDTL. In the second-generation power supply, each individual circuit consists of a switchable capacitor in line with a high voltage transformer; the arcing electrodes are connected to the secondary side of the coil. The capacitor is charged by a 100 V DC power supply when the first switch is closed and the second open; at the user-specified time the switches flip and it discharges through the coil. A schematic of the circuitry can be found in Figure 2. The switches are controlled by a 16-channel digital I/O card and National Instruments' Labview software, operated by a dedicated computer. The plasma generator provides independent control of the frequency, duty cycle/pulse width, and phase of each individual actuator (though not the amplitude). The pulse width was held constant at 7 μs, which was found to be the minimum pulse width at which the actuators consistently arced for all frequencies explored in this study[37]. The circuit is capable of operating at up to 100 kHz, though presently it is limited to 20 kHz due to thermal concerns. In the present work, the jet was excited at forcing Strouhal number, St_{DF} ($f_F D/U_j$), of 0.02 and 0.15 and an azimuthal mode of m = 0 (i.e., the eight LAFPAs are fired in phase). The very low forcing Strouhal number was chosen such that each individual structure would evolve independently from the subsequent and previous structures seeded by forcing as it advects through the shear layer region of the jet[10].

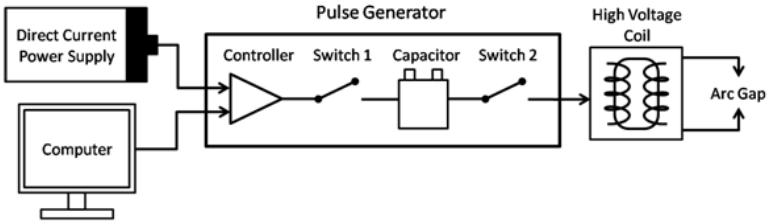

Figure 2: Schematic of the second-generation DC plasma power supply.

B. Data Acquisition

Near-field and far-field pressure measurements were acquired simultaneously, using Brüel & Kjær ¼ inch 4939 microphones. The signal from each microphone is band-pass filtered from 20 Hz to 100 kHz using a Brüel & Kjær Nexus 2690 conditioning amplifier, and recorded using National Instruments PXI-6133 A/D boards and LabView software. The microphones are calibrated using a Bruel & Kjaer 114 dB, 1 kHz sine wave generator. The frequency response of the microphones is flat up to roughly 80 kHz, with the protective grid covers removed. Voltage signals are collected at 200 kHz with 81920 data points per block; sub-blocks of 8192 data points were used when calculating short-time power spectral densities, resulting in a frequency resolution of 24.4 Hz. Ten blocks were recorded for each case resulting in four seconds of data, which has been found to be sufficient for convergence of turbulence statistics.

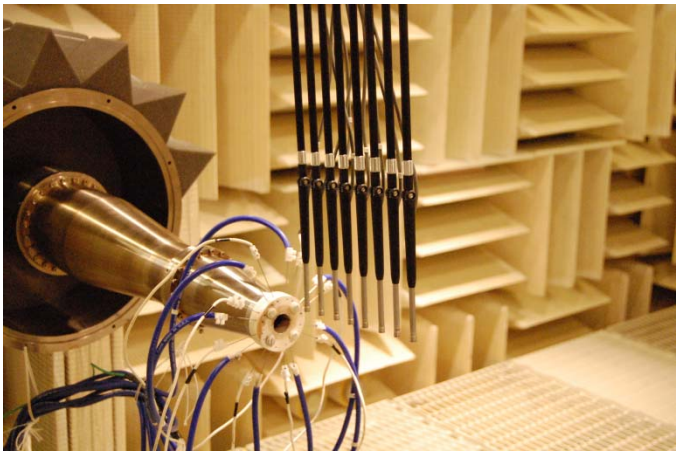

Figure 3: Photograph of anechoic chamber and nozzle, with near-field linear microphone array in foreground.

Far-field acoustic pressure was acquired at eleven polar angles spanning 25° to 120°, as measured from the downstream jet axis. The far-field microphone array is comprised of two linear sections running perpendicular to the jet axis which contain the upstream and downstream angle microphones, and a third linear section running parallel to jet for the sideline angle microphones (Figure 1). The microphones are oriented such that the normal vector from their tips intersects the jet downstream axis at the nozzle exit. The radial distance of the microphones ranges from $96.5D$ at 25° to $145D$ at 60°. The near-field pressure was acquired using an array of eight microphones, linearly spaced 2.54 cm (1 in.) apart and located along the meridional plane of the jet (Figure 3). The linear array was mounted on an x-y traverse system, which was controlled using Labview; the array was mounted at an angle of 8º to the jet axis in order to match the spreading angle of the jet shear layer for this Mach number, as determined via PIV during previous studies[7]. Initially, the most upstream microphone is positioned at $x/D = 2$ and $y/D = 1.28$, to ensure that the microphone tips are outside the mixing layer and do not affect the flow field. For subsequent cases, the microphone array was incremented radially outward by $0.2D$ for a total travel distance of $5D$, and incremented once axially by $0.5D$, for a total of 26 microphone locations in the radial direction and 16 in the axial direction. A schematic of the microphone locations can be found in Figure 4.

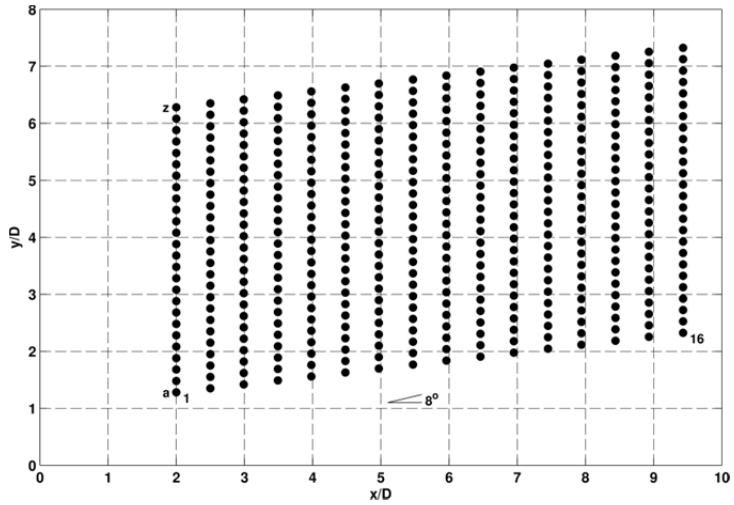

Figure 4: Microphone array coordinates for near-field measurements.

In the present work, the phase-averaging technique used in Sinha et al.[10] is employed in order to study the evolution of the seeded perturbations, both spatially and temporally. The TTL pulse sequence, which controls the LAFPAs, is supplied to an Agilent 3320A waveform generator. The rising edge of the TTL pulse triggers a sharp drop in the output voltage of the waveform generator, which then ramps back up to the original voltage over a time interval which is shorter than the minimum forcing period. The output from the waveform generator is acquired simultaneously with the near- and far-field pressure signals using the aforementioned National Instruments hardware and software. As the forcing frequency, azimuthal mode, and ramp signal are well defined, this system enables the identification of the zero phase of actuation and hence, the ability to phase-average the pressure signals over the forcing period. This ensures that the seeded perturbations can be readily identified in the noisy flow, as well as allowing pressure signals, which were not recorded simultaneously (i.e. different near-field array positions), to be analyzed concurrently.

Analysis of the near-field response of the forced jet is not immediately straightforward due to acoustic contamination from the actuators themselves[10]. LAFPAs operate on a joule heating principle - the breakdown of the air between the electrodes and the ensuing flow of current results in intense heating of the air. This rapid, localized thermal perturbation produces a compression wave, which excites the shear layer. However, this compression wave is still evident as it travels through the near field. Obviously, this is an undesirable effect, as this actuator self-noise may in some cases obscure the hydrodynamic and acoustic response of the jet. In the present work, the near-field pressure signals have been preprocessed using a continuous-wavelet-based filtering algorithm, which has been specifically designed to remove the actuator self-noise while leaving the response of the jet unaltered. Further details of the filtering algorithm and sample filtered and raw signals can be found in the references[38].

IV. Results

This work represents a continuation of the inquiry begun by Sinha et al.[10] and by Alkandry et al.[38] into the hydrodynamic and acoustic response of subsonic jets subjected to forcing. As such, the reader may benefit from a brief review of the findings which are pertinent to the present study. Further details may be found in the relevant works.

A. Hydrodynamic response of the jet to forcing

The hydrodynamic response of high Mach number, subsonic jets was studied by decomposing the periodically-forced near-field pressure into a wave and a residual components, as carried out by Hussain and Reynolds[39]. It was found that each plasma pulse produces a perturbation that gets amplified in the shear layer of the jet and rolls up into a large-scale structure; for the lowest forcing frequency explored in this study, these structures manifest as a compression wave closely followed by an expansion wave in the irrotational near field just outside the shear layer[10]. The duration of this event at the $x = 2D$ microphone, for example, is approximately $4D/U_j$. At a forcing Strouhal number of 0.02, the forcing period is significantly longer than the above time scale. Hence, the individual structures produced by the forcing evolve independently of one another as they advect through the shear layer past the end of the potential core. However, as St_{DF} is increased, the time between successive structures is reduced to the point where they begin interacting with each other as they evolve downstream. It was shown that this interaction is initially quasi-linear[10].

The behavior of the hydrodynamic response of the jet can be observed in Figure 5, where the phase-averaged waveforms for the two forcing Strouhal numbers explored in this study, 0.02 and 0.15, are shown at $x/D = 2$ and $x/D = 6$ along the first array position, which correspond to the most upstream microphone placement and the end of the potential core (as determined by previous studies[7]), respectively. Note the change in ordinate scale between the figures. For both St_{DF}, the compact response of the jet is evident at the most upstream microphone location: a compression wave trailed by an expansion wave of similar amplitude and duration. As discussed in Sinha et al.[10], the low-amplitude waves which precede the hydrodynamic response of the jet are the actuator "self-noise" which travel directly from the actuators to the microphones, unmodulated by the flow. It was found that the fundamental response of the jet was constant, so long as the forcing period was sufficiently long as to allow the jet to return to its natural state. As the forcing frequency was increased, the structures began to interact quasi-linearly. The forcing frequency at which this occurs is a function of the axial position, due to the growth of the generated structures. Here, it is observed that the compression wave is nearly identical in both shape and amplitude between the two waveforms at the most upstream location. Further downstream, near the end of the potential core, it is seen that the response of the jet for $St_{DF} = 0.02$ is not as compact as it was upstream, though the waveform still returns to the ambient pressure before the next forcing period. It is for this reason that this forcing Strouhal number will be referred to as the impulse-forced jet throughout this paper. On the other hand, for $St_{DF} = 0.15$ the waveform has been significantly modified from the fundamental response, both in compression and expansion amplitudes as well as shape. Throughout the rest of this work, $St_{DF} = 0.15$ will be referred to as the periodic-forced jet.

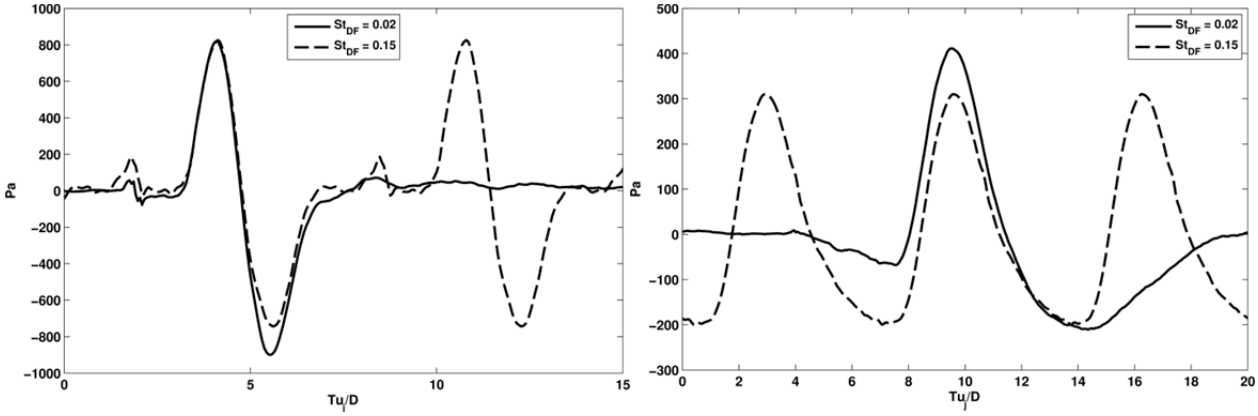

Figure 5: Phase-averaged waveforms at $x/D = 2.0$, $y/D = 1.3$ (left) and $x/D = 6.0$, $y/D = 1.8$ (right).

The effect of forcing on the pressure fluctuation intensity, P_{rms}, along the jet can be observed in Figure 6 and serves as a simple way of evaluating the large-scale structure dynamics. For the unforced jet the fluctuation intensity peaks at $x/D = 5$, which is just upstream of the end of the potential core, and slowly decays beyond that point. Forcing, either impulse or periodic, results in a significant amplification of the intensity peak, an upstream shift in

the saturation location (around x/D = 3.5 and x/D = 2.5 for the impulse and periodic forcing, respectively) and a much more marked decay rate downstream. For both jets, significant decay starts near x/D = 4. It is unsurprising that the periodic-forced has both a greater intensity and a greater decay rate than the impulse-forced jet. This is because the forcing produces large-scale structures which are more energetic and coherent than in the natural jet; during the impulse-forcing the jet returns to its unforced state for significant periods of time between the successive structures whereas this is not the case for the periodic-forced jet. The highly energetic, coherent vortex rings produced by the forcing also likely begin to self-interact near the jet centerline upstream of the time-averaged end of the potential core, producing an upstream shift in the saturation point. Previous experiments with forced jets found that the length of the potential core was noticeably shortened when forcing near the jet column instability with $m = 0$[6].

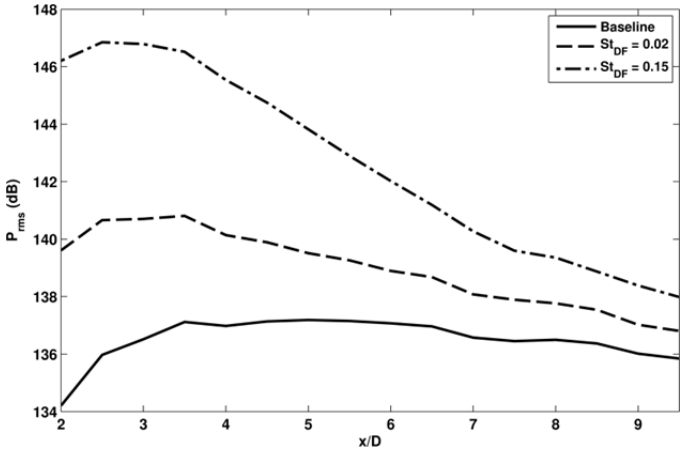

Figure 6: Pressure fluctuation intensity along the first array position.

B. Near-field autocorrelations

The autocorrelations of the near-field signals were investigated in order to gain a better understanding of the physical components of the irrotational pressure field. Sample autocorrelations are presented in Figure 7, where the normalized autocorrelations at x/D = 9 are shown for the first and last array positions; the trends observed in these plots are representative of those observed at other radial and axial positions. In these plots the autocorrelations have been computed for the forced jets using both the instantaneous waveforms (in which the wavelet-filtering has been performed, but no phase-averaging) as well as the phase-averaged waveform.

The autocorrelations for the instantaneous forced jets are found to be remarkably similar to that of the unforced jet at both radial locations, indicating that hydrodynamic and acoustic response of the jet is not being noticeably modified by the forcing. At locations near the jet shear layer, where the signature of the large-scale structures dominates, the instantaneous autocorrelations exhibit a wide half-width and a slightly negative trough. As the probe is traversed outwards radially, the shape of the autocorrelation function shifts to one with a significantly narrower half-width and no significant negative correlation regions, indicative of the acoustic signature from a range of turbulent scales (note that the polar angle for this location is approximately 60° from the jet centerline at the end of the potential core). Similar autocorrelation shapes have been found in far-field acoustic spectra by other researchers, who associated the negative correlation troughs with the acoustic signature of coherent large-scale structures[2].

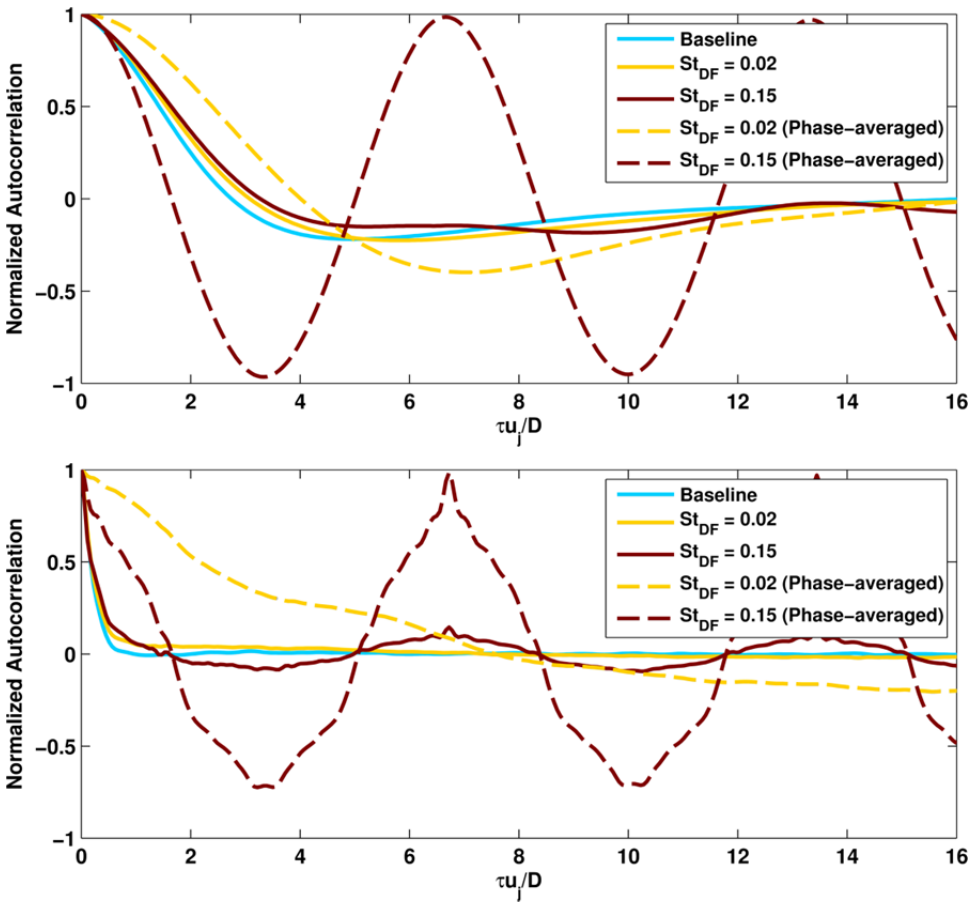

Figure 7: Normalized autocorrelations at *x/D* = 9 along the first array position (top) and last array position (bottom).

The behavior of the autocorrelations changes dramatically when the phase-averaged waveforms are used in place of the instantaneous. At the first array position, the phase-averaging results in deeper correlation troughs as well as correlation half-widths that are dissimilar to the unforced jet, with the periodic-forced jet exhibiting narrower half-widths than the unforced jet and the impulse-forced jet exhibiting wider. This is expected since the hydrodynamic signature is exclusively that of low frequency, high wavelength for the impulse response and higher frequency, lower wavelength for the periodic response. In the unforced jet, the signature produced by a wide range of large scales and low wavelengths, with a mean falling in between St = 0.02 and 0.15. An interesting and surprising result is observed as the microphones are traversed radially outwards: the autocorrelations do not shift to the narrow half-widths, but retain the essential features of the large-scale structure-dominated signals observed at the first array position. In the case of the periodic-forced jet, the autocorrelations are nearly identical in half-width and negative correlation amplitude at both array positions, the only difference being small amplitude oscillations of no discernible fundamental frequency (it was observed that the signal-to-noise ratio of the phase-averaged waveform decreases at further array positions). For the impulse-forced jet, the half-width actually increases with radial distance, contrary to what was observed for the instantaneous signals. Assuming noise generated by a structure with frequency f in the impulse forcing case retains the frequency, the wavelength increases when the energy transitions from hydrodynamic to acoustic, which is what the phase-averaged autocorrelations indicate. A similar argument cannot be made with the periodic forcing case, as the structures are interacting and complicating the picture. Similar results are obtained at upstream axial locations for both the first and last array positions, which for brevity will not be shown here. While further investigation of these results is forthcoming, it is clear that the structures generated by forcing (both impulse and periodic) *are producing coherent radiation, which is phase-locked to the structures and hence can be recovered by the phase-averaging*.

C. Near-field to far-field correlations

Further information regarding the noise generation process from the large-scale structures may be obtained by analyzing the two-point correlations from the near-field to the far-field microphones. The correlations along the first array position to the far field at 30° have been plotted in Figure 8 for the forced and unforced jets computed from the instantaneous signals. In the case of the unforced jet, two distinct positive correlation peaks are observed at each axial location, along with a single negative correlation peak. The maximum correlation amplitude increases with downstream distance, reaching a maximum of just under 0.2 at the furthest axial position explored in this study. Similar correlation values have been obtained by other researchers in unforced jets[40]; it was also found that the peak correlation values occurred downstream of the end of the potential core[40,41]. However, the maximum correlation amplitude does not occur at the same positive correlation peak at all axial locations; in the upstream region the maximum correlation is obtained on the trailing positive peak whereas it occurs on the leading peak in the downstream region. A quick note should be made for clarification purposes: the trailing peak corresponds to an event that occurs later in time. Hence, it takes less time for the event to reach the far-field reference microphone, and thus produces a correlation peak at smaller time delay. The opposite is true for the leading correlation peak. While the leading positive peaks exhibits monotonic growth with axial distance, the trailing positive peaks grows until $x/D = 5$, after which it begins to decay. Similarly, the negative correlation peaks exhibit both growth and decay, though in this case the maximum negative peak occurs at $x/D = 7$. While it is not yet clear to what physical phenomena these peaks correspond to, this behavior is highly suggestive of separate flow phenomena (this will be further investigated in §IV.D below).

The near-field to far-field correlations along the first array position for the impulse-forced jet are found to be quite similar to those of the unforced jet. Two positive correlation regions are found to be separated by a negative correlation region, the maximum correlation value is again found at the most downstream microphone location, and the maximum correlation value does not occur at the same positive correlation peak at all axial locations. Minor differences in shape and amplitude do exist, but the greatest positive correlation peaks are nearly identical, particularly at the downstream locations. On the other hand, periodic-forcing has significantly altered both the shape and amplitudes of the correlations. The curves appear sinusoidal over the entire domain, and peak further upstream, near the end of the potential core, and decay significantly beyond that point. The sinusoidal shape of the correlations is of course expected, and matches the forcing frequency. It should be noted that the correlations for the impulse-forced jet also exhibit the expected periodicity, though it is not apparent in Figure 8 due to the range over which the curves have been plotted.

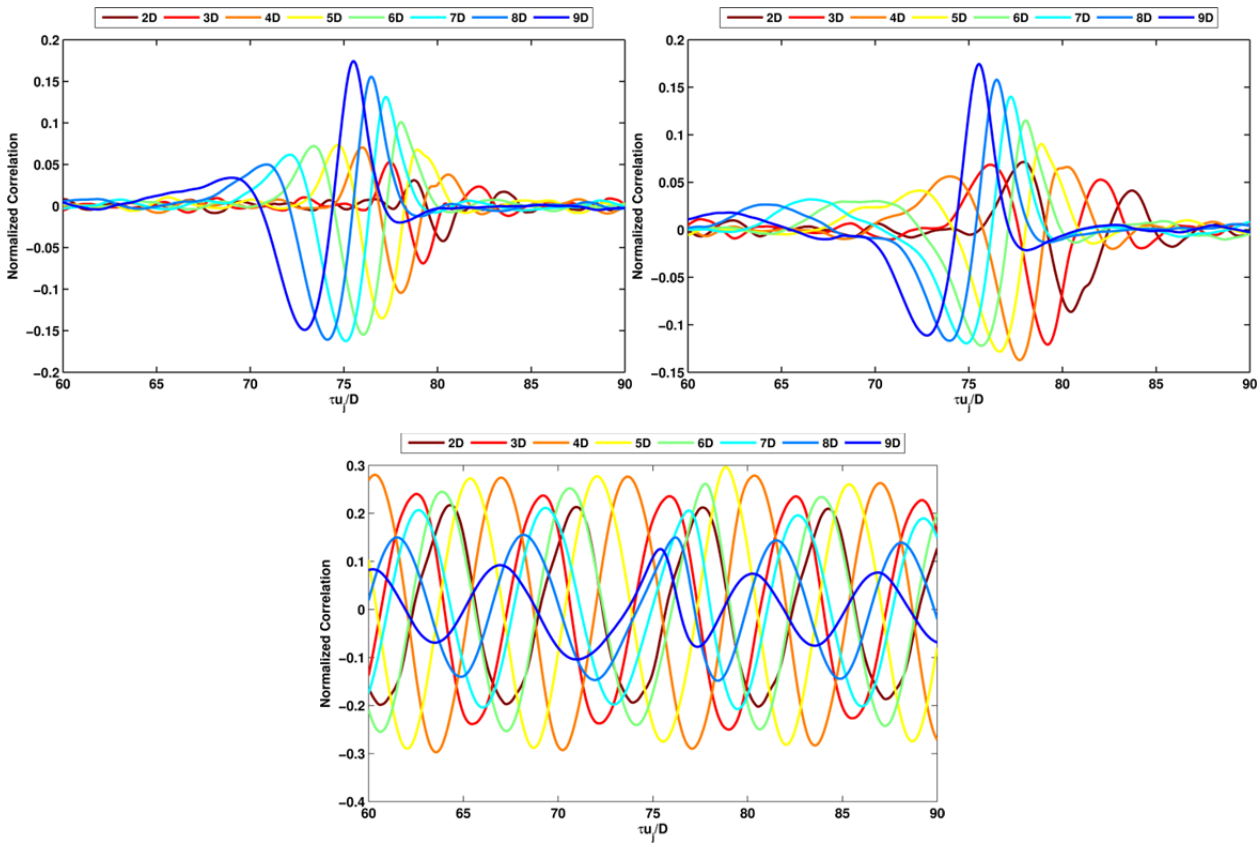

Figure 8: Instantaneous cross-correlations to 30° far field along the first array position for unforced (top left), St_{DF} = 0.02 (top right), and St_{DF} = 0.15 (bottom) forced jets.

In Figure 9 the maximum correlation value to the far field at 30° has been plotted for all near-field microphone locations explored for the forced and unforced jets. Clearly, the maximum correlation is a function of both axial and radial positioning of the near-field microphone. Given the previous results discussed, it is unsurprising that the correlation map for the impulse-forced jet is nearly identical to that of the unforced jet. In the case of these jets, the maximum correlation to the downstream polar angles is practically zero for the upstream near-field positions, particularly at large radial distances. This is to be expected, as previous researchers have shown that radiation from the large-scale structures radiate is preferentially to the downstream angles. The radiation to sideline angles has been shown to be dominated by small-scale structures, which are incoherent[2]. As expected, the greatest correlation values are observed in the downstream direction, in this case at roughly 3*D* radially outwards from the jet centerline. The line connecting the peak near-field correlation location with the far-field microphone at 30° crosses the jet centerline at roughly x/D = 4, which corresponds to the location of significant P_{rms} decay in the forced jets (see Figure 6). The significance of this will be discussed in further detail in the next section. Based on these results, it can be concluded that the structures generated by the impulse-forcing are not significantly changing either the hydrodynamic or acoustic response of the natural jet. For the periodic-forced jet, the normalized correlation values have been significantly enhanced over the unforced jet. This is most noticeable in the upstream region of the jet near the shear layer, though the peak correlation value in the downstream region has also been enhanced. However, it is not yet clear from these plots to what the far-field signal is correlating, nor how (or if) the noise generation process from the large-scale structures has been affected.

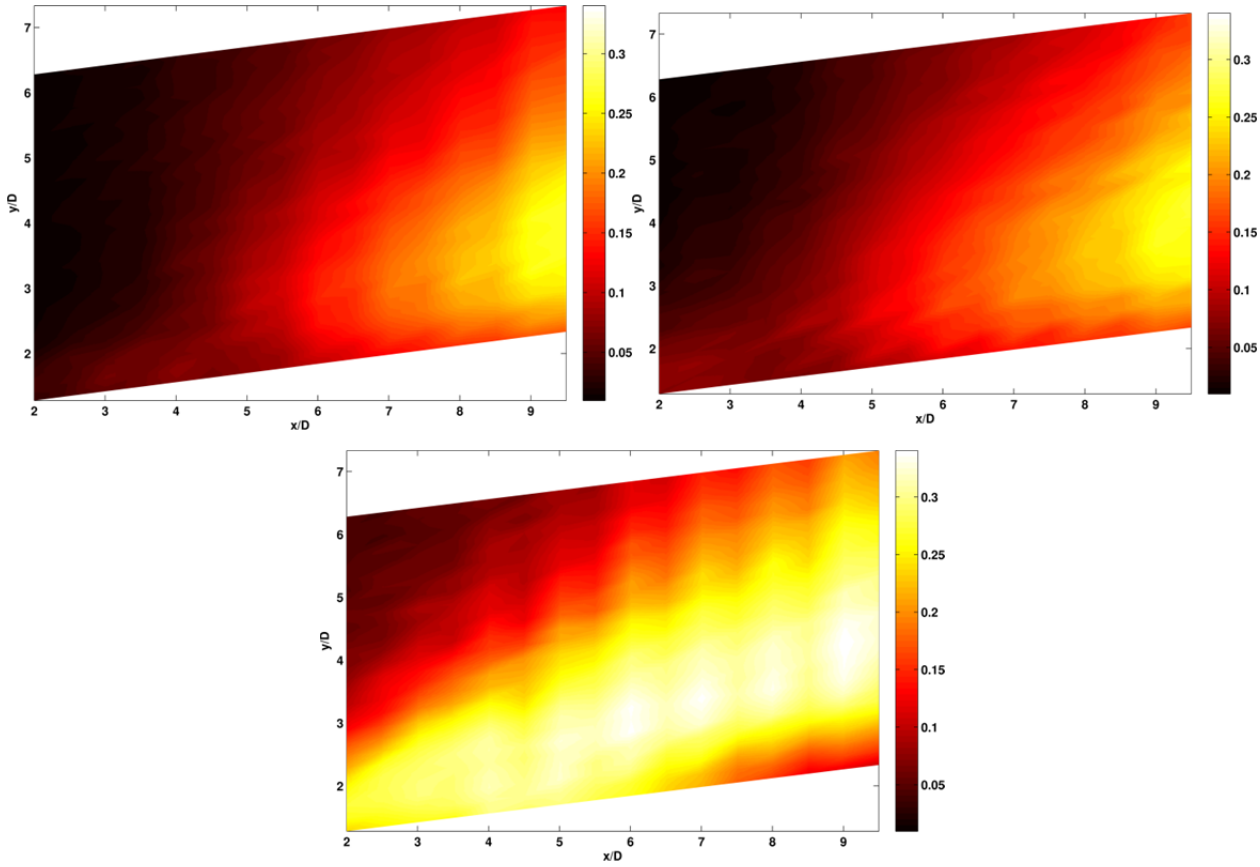

Figure 9: Maximum correlation to far field 30° for unforced (top right), St_{DF} = 0.02 (top left), and St_{DF} = 0.15 (bottom) jets.

D. Spatio-temporal evaluation of the near field to far field correlations

In this section, the near-field to far-field correlations presented previously are analyzed in the spatio-temporal domain. The correlation regions are then compared with two expected time lags, as defined similarly by other researchers[42]. The first, τ_{ac}, corresponds to the expected time lag for an acoustic wave traveling directly from the noise source to the near-field microphone and on to the far-field microphone. The second, τ_{con}, corresponds to the expected time lag for a large-scale structure to convect to the acoustic source region and radiate acoustically to the far-field microphone. In this case, the convective velocity was assumed to be $U_c = 0.65U_j$ (as determined by two-point correlations between neighboring near-field microphones outside the potential core region of the jet) and the acoustic source region was assumed (somewhat arbitrarily) to be located at $x_s/D = 4$ (this value was chosen to best match the observations made subsequently, it was also observed to be the location at which significant P_{rms} decay occurs in the forced jets) along the jet centerline. A schematic of the propagation paths for the two expected time lags can be found in Figure 10. It should be noted that although the near-field and far-field microphone arrays are not at the same azimuthal angle with respect to the nozzle, the computations for the expected time lags do not account for this difference. It has been assumed that the acoustic radiation in jet is dominated by $m = 0$ azimuthal Fourier mode. This assumption is easily justifiable in the forced jets, where the actuators have been fired in phase. While the near-field pressure and acoustic radiation towards aft polar angles in a natural, high Reynolds number jet is a combination of numerous azimuthal Fourier modes, previous researchers have found these fields to be dominated by the axisymmetric Fourier mode[4,43-45]. Hence, the authors feel the assumption of axisymmetric noise sources and radiation is also valid in the unforced jet as well.

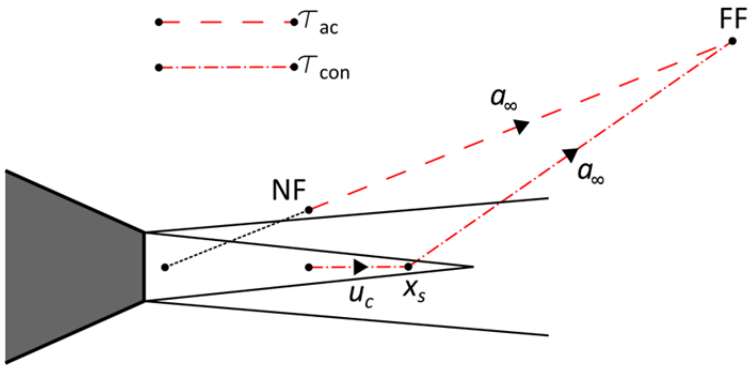

Figure 10: Schematic of propagation paths for expected time of arrivals (not to scale).

The space-time correlations for the unforced jet along two array positions to the far field at 30° are shown in Figure 11. Note that the ordinate in the figures has been non-dimensionalized by the ambient speed of sound, a_∞, and *R,* the distance from the near-field microphone to the far-field microphone, while the abscissa has been non-dimensionalized by *D*, the nozzle exit diameter. In the location closest to the jet, two strong positive correlation regions are separated by one strong negative region. The estimated time-of-arrival for an acoustic wave lines up well with the leading positive correlation region downstream of the potential core. The trailing positive region as well as the negative region exhibit slower propagation velocities, with the trailing positive region matching well with the assumed convective velocity of the large-scale structures. Upstream of roughly $x/D = 5$, the amplitude of the correlations is significantly lower. The strongest correlation region starts from almost negligible values further upstream, and strongly amplifies beyond the end of the potential core, while the negative and trailing positive correlations only grow moderately. Additionally, the locations of the maxima for each region are not the same: for the strong-positive and negative regions the maxima occur near the end of the domain while the maximum for the weak-negative region occurs near the end of the potential core ($4 < x/D < 7$). As the microphone array is moved radially outwards, the trailing positive region quickly decays to negligible values. This, coupled with the previous observations, strongly indicates that these positive correlation regions correspond to distinct flow phenomena. Upstream of the source location, the positive correlation region appears to be associated with the braid region of the large-scale structure as it convects through the shear layer. The negative region corresponds to the low pressure core region of the vortex. As the structures approach the source region and likely begin to interact, acoustic radiation is generated, and both the negative and positive correlation regions shift to an acoustic propagation velocity.

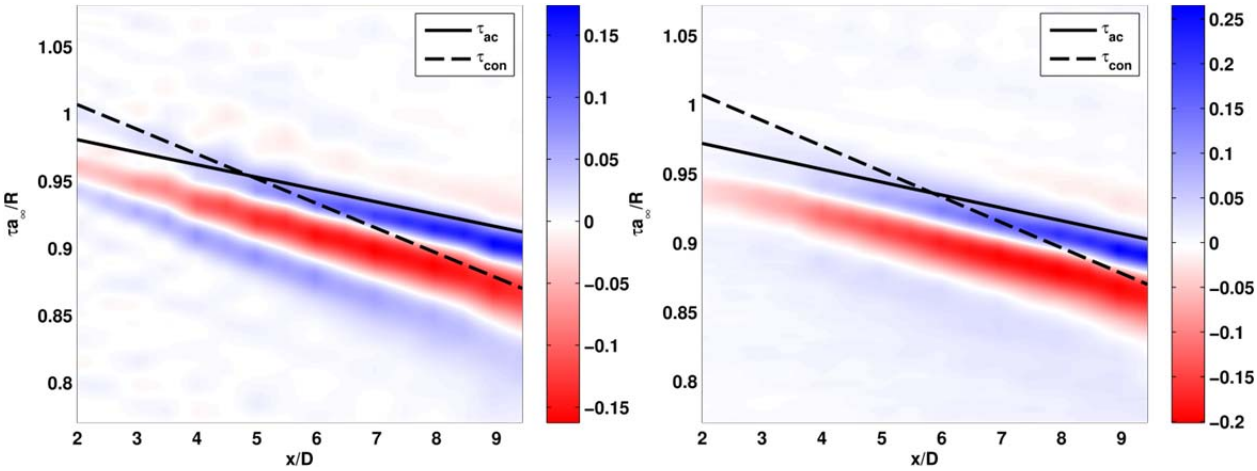

Figure 11: Normalized cross-correlations to the far field at 30° for *y/D* = 1.28 (left) and *y/D* = 3.08 (right) in the unforced jet.

In Figure 12, the space-time correlations between the first microphone array position and the far field at 30° have been plotted for the impulse- and periodic-forced jets. Similar to the unforced jet cross-correlations to this polar angle, two strong positive and one strong negative correlation regions are observed in the impulse-forcing. The estimated time-of-arrival for an acoustic wave lines up well with the leading positive correlation region (which again

is also the strongest region) in the region downstream of the end of the potential core. As with the unforced jet, the locations of the maxima for each region are not the same: for the leading positive region the maximum occurs near the end of the domain while the maximum for the trailing positive region occurs in the jet core region; the negative correlation region is relatively consistent in amplitude over the entire domain, with a slight peak near the end of the potential core. In the core region of the jet, the apparent propagation velocities of the correlation regions shift to a significantly lower speed than the ambient speed of sound, and match well with the convective propagation velocity. Also unlike the unforced jet, the leading positive correlation region in the forced jet extends over the entire domain, and the trailing positive correlation region decays much more quickly with axial distance.

Unlike in the unforced or impulse-forced jet, in the periodic-forcing case, one distinct positive and negative correlation region is produced per forcing period. For both positive and negative regions, the maximum correlation is found to be located $4 < x/D < 6$, which corresponds to the end of the potential core. Upstream of this location, the correlation regions are found to match well with the convective estimated time-of-arrival while downstream of the end of the potential core the correlation regions match well with the acoustic propagation path. While the absence of the trailing positive region that is seen in the unforced and impulse-forced jets is a major difference, the behavior of the positive and negative correlation regions for the periodic-forced jet are again quite similar to the unforced and impulse-forced jets. The trends observed in this figure are suggestive of a coherent structure which convects through the shear layer in the jet core region and produces noise (likely due to interaction) that radiates to the far-field just upstream of or at the end of the potential core. Similar behavior has been observed numerically[42]. The behavior remains unchanged by the quasi-linear interaction of the large-scale structures (in the periodic-forced jet), or the upstream shift in the saturation point for the forced jets over the unforced jet.

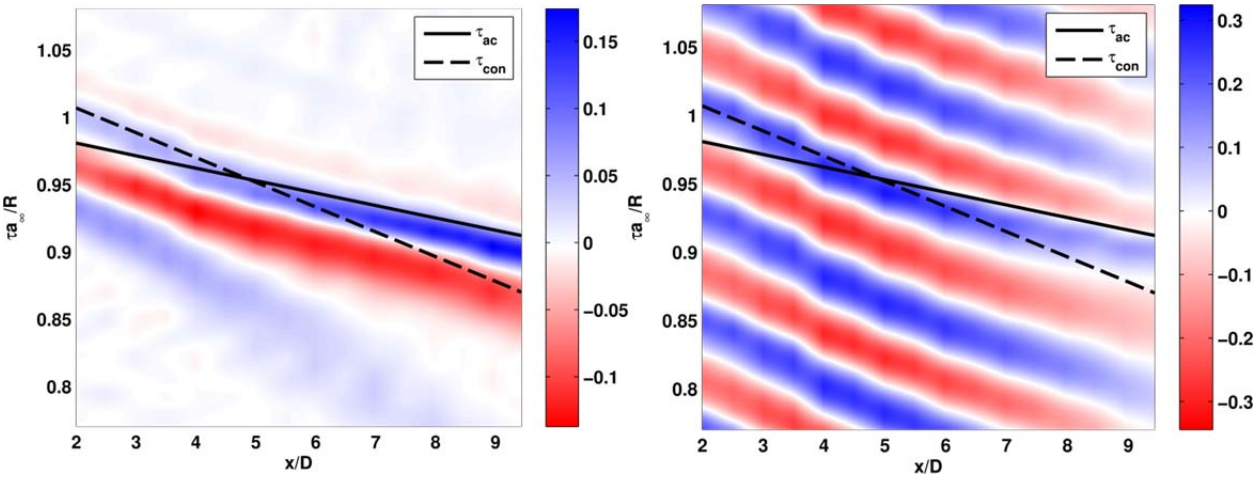

Figure 12: Normalized cross-correlation along the first array position to the far field at 30° for St_{DF} = 0.02 (left) and St_{DF} = 0.15 (right).

The existence of two positive correlation regions, as well as a negative correlation region which appears to share characteristics with both of the positive correlation regions, is somewhat perplexing. These behaviors may be explained by the characteristic shape of the phase-averaged impulse response of the jet in the far field at a polar angle of 30°, as shown in Figure 13. It has been shown[46] that the reactive and propagative pressures are out of phase by $\pi/2$, however the signal inversion that the disturbance has undergone as it traveled from the near field to the far field is surprising (the reader is referred back to Figure 5 for the corresponding near-field waveforms). An additional low-amplitude positive excursion is also observed to be following the primary compression wave in the far field. Clearly, the spectral content and phase of the reactive and propagative pressures are significantly different. The purely acoustic wave in the far field will correlate to both the hydrodynamic and the acoustic components in the near field, due to the conformity of the spectral contents and phase, though this will not necessarily occur at the same time lags. Further inquiry into the behavior of the correlation regions is ongoing.

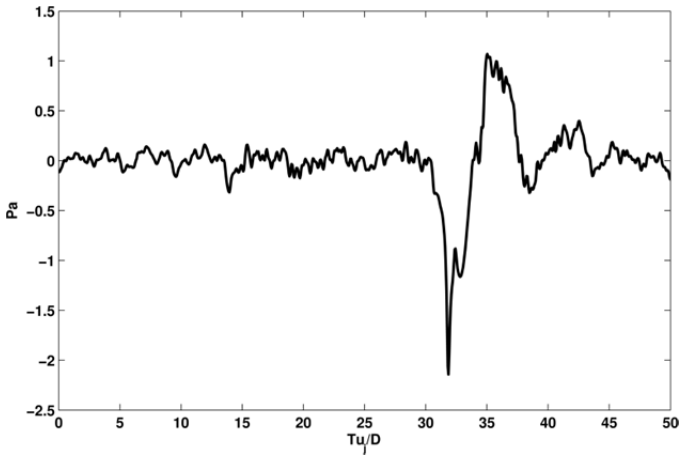

Figure 13: Impulse response at 30° far field.

As the far-field reference microphone is shifted to larger polar angles, the behavior of the space-time correlations begins to change. In Figure 14, the normalized correlations along the first array position to the far field at 60° have been plotted for the unforced and impulse-forced jets. Here, there is one (relatively) strong positive correlation region which matches well with the expected time-of-arrival for an acoustic wave and which exists over the entire domain. However, alternating regions of lower-amplitude positive and negative correlations exist for other lag times, primarily in the core region of the jet. The apparent propagation velocity of these regions matches well with the convective velocity. The correlations to the far field at 60° along further radial positions do not exhibit alternating positive and negative regions which match the convective velocity of the large-scale structures, though for brevity they will not be shown here. The behavior in these plots is suggestive of coherent structures that are generating radiation to 60° far-field over the entire domain observed in this study. The alternating positive and negative correlation regions correspond to the large-scale structures themselves (rather than acoustic radiation).

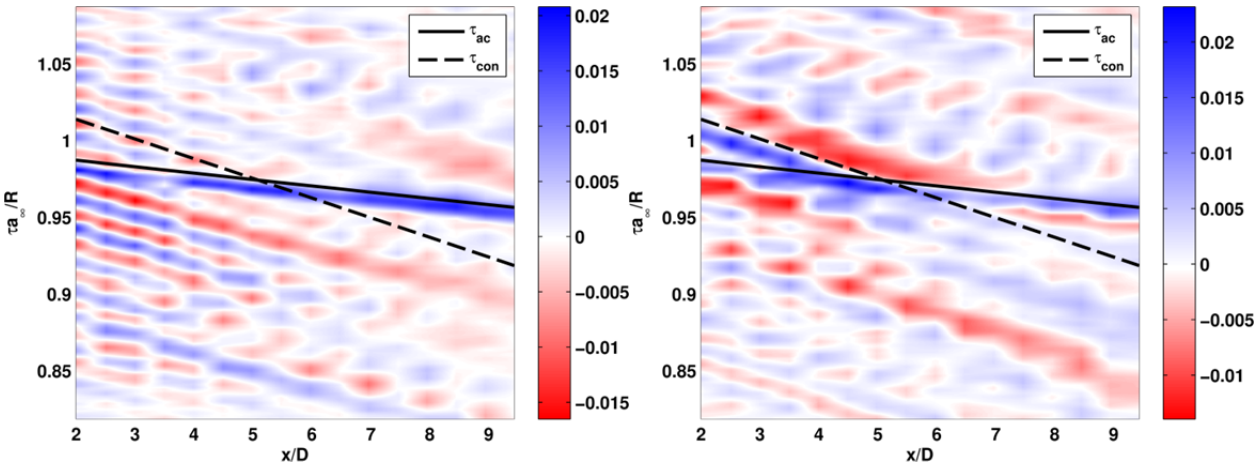

Figure 14: Normalized cross-correlation along first array position to far field at 60° for unforced (left) and St_{DF} = 0.02 (right) jets.

For the periodic-forced jet correlations to the far field at 60°, shown in Figure 15, continuously-oscillating correlation regions are again observed, though with much lower amplitude than previously, with the highest correlation levels occurring in the jet potential core region and decaying downstream. This is as one would expect, as the radiation to this polar angle is composed of sources from various levels of coherence. Close to the jet shear layer, the correlation regions do not match with the estimated time-of-arrival for an acoustic wave at any location inside the measurement domain. Rather, the regions match the convective propagation velocity. In this case, the hydrodynamic signature of the large-scale structures is overwhelming the correlations to the acoustic signature. This can be seen by comparing to the correlations along the last array position. At the furthest array position, it is observed that the acoustic radiation towards this polar angle occurs over the entire domain, similar to the unforced and impulse-forced jets.

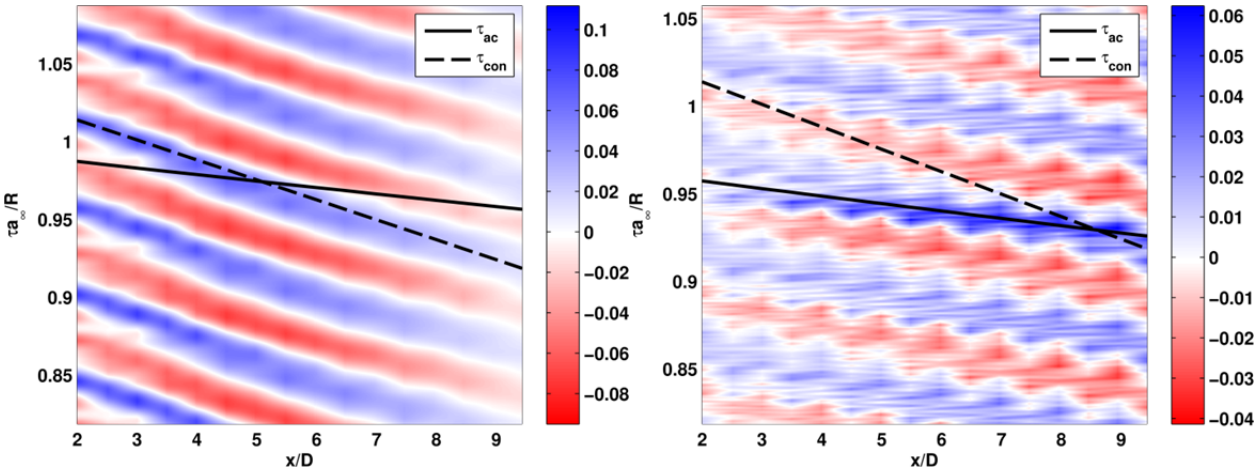

Figure 15: Normalized cross-correlations to far field at 60° along first array position (left) and last array position (right) for St_{DF} = 0.15 forced jet.

V. Conclusions

The actuators used in this study provide a unique opportunity to investigate the dynamics of large-scale structures, the noise sources, and the radiated noise; the well-defined actuation phase enables phase-averaging of the pressure signal. Hence, time-resolved (more precisely phase-resolved) measurements over an entire region of the near-field may be acquired and correlated, providing additional insight into the noise sources than the conventional two-point correlations. By acquiring and processing both the near-field and far-field pressure/acoustic signals in this fashion, noise events in the far field and the region from which they emanate may be located.

Results show that *the forcing produces coherent, large-scale structures which generate coherent radiation to the far field*. When forcing at very low frequencies (impulse), the structures evolve independently as they advect through the shear layer. When forcing at moderate frequencies (periodic), the structures interact quasi-linearly. The acoustic radiation produced by the large-scale structures (generated by the forcing) is observed to be coherent at aft angles to 60° polar angle. This becomes evident when the signals are phase-averaged to remove the incoherent sources which typically dominate the radiation towards the sideline angles. Forcing the jet in the periodic regime modifies the near-field to far-field cross-correlations by enhancing the coherence of the large-scale structures and the generated noise to the far field. However, it was found that forcing, either impulse or periodic, did not affect the sound source statistics or source region. The disintegration of the structures as they pass through the end of the potential core has been suggested as a source mechanism for downstream acoustic radiation[47]; the results of this study also point towards this mechanism as being the dominant noise source towards the downstream polar angles in this jet.

This work represents another step in an ongoing inquiry into the hydrodynamic and acoustic response of high speed, high Reynolds number jets to the generation of large-scale structures. As such, a more complete characterization of the linear and nonlinear interaction of the large-scale structures, and their effect on the far-field acoustic radiation, is underway. Additionally, the microphone array grid will be extended axially downstream, the result of which will be twofold. First, this will better capture the radiation to the downstream polar angles which is originating near the end of the potential core. Second, this will enhance the wavenumber resolution of the array, allowing the decomposition of the waves into their constitutive hydrodynamic and acoustic components based on the measured phase velocities.

Acknowledgements

The authors would like to acknowledge Dr. Martin Kearney-Fischer for his insight into wavelet-based filtering and fruitful discussions. The support of this work by the Air Force Office of Scientific Research (Dr. John Schmisseur and Dr. Rengasamy Ponnappan) is appreciated.

References

[1]Lighthill, M. J., "On Sound Generated Aerodynamically. I. General Theory," *Proceedings of the Royal Society of London: Series A, Mathematical and Physical Sciences*, Vol. 211, The Royal Society, 1952, pp. 564-587

[2]Tam, C. K. W., Viswanathan, K., Ahuja, K. and Panda, J., "The Source of Jet Noise: Experimental Evidence," *Journal of Fluid Mechanics*, Vol. 615, 2008, pp. 253-292.

[3]Jordan, P. and Colonius, T., "Wave Packets and Turbulent Jet Noise," *Annual Review of Fluid Mechanics*, Vol. 45, 2013, pp. 173-195.

[4]Arndt, R. E. A., Long, D. F. and Glauser, M. N., "The proper orthogonal decomposition of pressure fluctuations surrounding a turbulent jet," *Journal of Fluid Mechanics*, Vol. 340, 1997, pp. 1-33.

[5]Suzuki, T. and Colonius, T., "Instability waves in a subsonic round jet detected using a near-field phased microphone array," *Journal of Fluid Mechanics*, Vol. 565, 2006, pp. 197-226.

[6]Samimy, M., Kim, J. H., Kastner, J., Adamovich, I. and Utkin, Y., "Active Control of High-Speed and High-Reynolds-Number Jets Using Plasma Actuators," *Journal of Fluid Mechanics*, Vol. 578, No. 1, 2007, pp. 305-330.

[7]Kearney-Fischer, M., Kim, J.-H. and Samimy, M., "Control of a high Reynolds number Mach 0.9 heated jet using plasma actuators," *Physics of Fluids*, Vol. 21, 2009, pp. 095101.

[8]Kim, J.-H. and Samimy, M., "Effects of Active Control on the Flow Structure in a High Reynolds Number Supersonic Jet," *International Journal of Flow Control*, Vol. 1, No. 2, 2009, pp. 99-117.

[9]Samimy, M., Kim, J.-H., Kearney-Fischer, M. and Sinha, A., "Acoustic and flow fields of an excited high Reynolds number axisymmetric supersonic jet," *Journal of Fluid Mechanics*, Vol. 656, 2010, pp. 507-529.

[10]Sinha, A., Alkandry, H., Kearney-Fischer, M., Samimy, M. and Colonius, T., "The impulse response of a high-speed jet forced with localized arc filament plasma actuators," *Physics of Fluids*, Vol. 24, 2012, pp. 125104.

[11]Tam, C. K. W. and Chen, P., "Turbulent Mixing Noise From Supersonic Jets," *AIAA Journal*, Vol. 32, No. 9, 1994, pp. 1774-1780.

[12]Tam, C. K. W., "Supersonic Jet Noise," *Annual Review of Fluid Mechanics*, Vol. 27, 1995, pp. 17-43.

[13]Kearney-Fischer, M., Kim, J.-H. and Samimy, M., "A Study of Mach Wave Radiation Using Active Control," *Journal of Fluid Mechanics*, Vol. 681, 2011, pp. 261-292.

[14]Tam, C., "Mach Wave Radiation from High-Speed Jets," *AIAA Journal*, Vol. 47, No. 10, 2009, pp. 2440-2448.

[15]Crow, S. C. and Champagne, F. H., "Orderly Structure in Jet Turbulences," *Journal of Fluid Mechanics*, Vol. 48, No. 3, 1971, pp. 547-591.

[16]Kibens, V., "Discrete Noise Spectrum Generated by an Acoustically Excited Jet," *AIAA Journal*, Vol. 18, No. 4, 1980, pp. 434-441.

[17]Zaman, K. B. M. Q. and Hussain, A. K. M. F., "Vortex pairing in a circular jet under controlled excitation. Part 1. General jet response," *Journal of Fluid Mechanics*, Vol. 101, No. 3, 1980, pp. 449-491.

[18]Gutmark, E. and Ho, C.-M., "Preferred modes and the spreading rates of jets," *Physics of Fluids*, Vol. 26, No. 10, 1983, pp. 2932-2938.

[19]Ho, C.-M. and Huerre, P., "Perturbed free shear layers," *Annual Review of Fluid Mechanics*, Vol. 16, 1984, pp. 365-424.

[20]Cohen, J. and Wygnanski, I., "The evolution of instabilities in the axisymmetric jet. Part 1 the linear growth of disturbances near nozzle," *Journal of Fluid Mechanics*, Vol. 176, 1987, pp. 191-219.

[21]Cohen, J. and Wygnanski, I., "The evolution of instabilities in the axisymmetric jet. Part 2 The Flow resulting from the interaction between two waves," *Journal of Fluid Mechanics*, Vol. 176, 1987, pp. 221-235.

[22]Samimy, M., Kim, J. H., Kastner, J., Adamovich, I. and Utkin, Y., "Active Control of a Mach 0.9 Jet for Noise Mitigation Using Plasma Actuators," *AIAA Journal*, Vol. 45, No. 4, 2007, pp. 890-901.

[23]Samimy, M., Zaman, K. B. M. Q. and Reeder, M. F., "Effect of Tabs on the Flow and Noise Field of an Axisymmetric Jet," *AIAA Journal*, Vol. 31, No. 4, 1993, pp. 609-619.

[24]Zaman, K. B. M. Q., Reeder, M. F. and Samimy, M., "Control of an axisymmetric jet using vortex generators," *Physics of Fluids*, Vol. 6, No. 2, 1994, pp. 778-793.

[25]Jubelin, B., "New Experimental Studies on Jet Noise Amplification," *AIAA 6th Aeroacoustics Conference* 1980-0961, 1980.

[26]Lu, H. Y., "Effect of Excitation on Coaxial Jet Noise," *AIAA Journal*, Vol. 21, No. 2, 1983, pp. 214-220.

[27]Ahuja, K. K. and Blakney, D. F., "Tone Excited Jets, Part IV: Acoustic Measurements," *Journal of Sound and Vibration*, Vol. 102, No. 1, 1985, pp. 93-117.

[28]Ahuja, K. K., Whipkey, R. R. and Jones, G. S., "Control of turbulent boundary layer flows by sound," *AIAA 8th Aeroacoustics Conference* 1983-0726, 1983.

[29]Samimy, M., Adamovich, I., Webb, B., Kastner, J., Hileman, J., Keshav, S. and Palm, P., "Development and characterization of plasma actuators for high-speed jet control," *Experiments in Fluids*, Vol. 37, No. 4, 2004, pp. 577-588.
[30]Utkin, Y. G., Keshav, S., Kim, J.-H., Kastner, J., Adamovich, I. V. and Samimy, M., "Development and use of localized arc filament plasma actuators for high-speed flow control," *Journal of Physics D: Applied Physics*, Vol. 40, No. 3, 2007, pp. 685-694.
[31]Kim, J. H., Kastner, J. and Samimy, M., "Active Control of a High Reynolds Number Mach 0.9 Axisymmetric Jet," *AIAA Journal*, Vol. 47, No. 1, 2009, pp. 116-128.
[32]Kearney-Fischer, M., Kim, J. H. and Samimy, M., "Flow Control of a High Reynolds Number Mach 1.3 Heated Jet Using Plasma Actuators," *AIAA 5th Flow Control Conference* 2010-4418, 2010.
[33]Kearney-Fischer, M. and Samimy, M., "Noise Control of a High Reynolds Number Mach 1.3 Heated Jet Using Plasma Actuators," *AIAA 48th Aerospace Sciences Meeting* 2010-13, 2010.
[34]Kim, J.-H., Kearney-Fischer, M., Samimy, M. and Gogineni, S., "Far-field Noise Control in Supersonic Jets Using Conical and Contoured Nozzles," *ASME Journal of Engineering for Gas Turbine and Power*, Vol. 133, 2011, pp. 081201.
[35]Samimy, M., Kearney-Fischer, M., Kim, J.-H. and Sinha, A., "High-Speed and High-Reynolds-Number Jet Control Using Localized Arc Filament Plasma Actuators," *Journal of Propulsion and Power*, Vol. 28, No. 2, 2012, pp. 269-280.
[36]Hahn, C., "Design and Validation of the New Jet Facility and Anechoic Chamber," M.S. Thesis, Mechanical Engineering, The Ohio State University, Columbus, OH, 2011
[37]Hahn, C., Kearney-Fischer, M. and Samimy, M., "On factors influencing arc filament plasma actuator performance in control of high speed jets," *Experiments in Fluids*, Vol. 51, No. 6, 2011, pp. 1591-1603.
[38]Alkandry, H., Crawley, M., Sinha, A., Kearney-Fischer, M. and Samimy, M., "An Investigation of the Irrotational Near Field of an Excited High-Speed Jet," *51st AIAA Aerospace Sciences Meeting* AIAA 2013-0325, 2013.
[39]Hussain, A. K. M. F. and Reynolds, W. C., "The mechanics of an organized wave in turbulent shear flow," *Journal of Fluid Mechanics*, Vol. 41, 1970, pp. 241-258.
[40]Hall, J. W., Hall, A. M., Pinier, J. T. and Glauser, M. N., "Cross-Spectral Analysis of the Pressure in a Mach 0.85 Turbulent Jet," *AIAA Journal*, Vol. 47, No. 1, 2009, pp. 54-59.
[41]Viswanathan, K., Underbrink, J. R. and Brusniak, L., "Space-Time Correlation Measurements in Nearfields of Jets," *AIAA/CEAS 16th Aeroacoustics Conference* 2010-3784, 2010.
[42]Bogey, C. and Bailly, C., "An analysis of the correlations between the turbulent flow and the sound pressure fields of subsonic jets," *Journal of Fluid Mechanics*, Vol. 583, 2007, pp. 71-97.
[43]Hall, J. W., Pinier, J., Hall, A. e. and Glauser, M., "Two-point correlations of the near and far-field pressure in a transonic jet," *ASME 2006 Joint U.S. European Fluids Engineering Summer Meeting* FEDSM2006-98458, 2006.
[44]Kœnig, M., Cavalieri, A. V. G., Jordan, P. and Gervais, Y., "Intermittency of the azimuthal components of the sound radiated by subsonic jets," *AIAA/CEAS 17th Aeroacoustics Conference* 2011-2746, 2011.
[45]Juve, D., Sunyach, M., and Comte-Bellot, G. , "Filtered Azimuthal Correlations in the Acoustic Far Field of a Subsonic Jet," *AIAA Journal*, Vol. 17, No. 1, 1979, pp. 112-113.
[46]Coiffet, F., Jordan, P., Delville, J., Gervais, Y. and Ricaud, F., "Coherent structures in subsonic jets: a quasi-irrotational source mechanism?," *International Journal of Aeroacoustics*, Vol. 5, No. 1, 2006, pp. 67 - 89.
[47]Hileman, J. I., Thurow, B. S., Caraballo, E. J. and Samimy, M., "Large-scale structure evolution and sound emission in high-speed jets: real-time visualization with simultaneous acoustic measurements," *Journal of Fluid Mechanics*, Vol. 544, 2005, pp. 277-307.